Rare Metal Materials and Engineering
Volume 51, Issue 8, August 2022
Available online at www.rmme.ac.cn

Science Press

Cite this article as: Wang Yujiao, Zhang Yun, Jiang Haitao, et al. Corrosion Behavior of Ca and Y Micro-alloyed Mg-2Zn-1Al Alloy[J]. Rare Metal Materials and Engineering, 2022, 51(08): 2777-2784.

ARTICLE

Corrosion Behavior of Ca and Y Micro-alloyed Mg-2Zn-1Al Alloy

Wang Yujiao, Zhang Yun, Jiang Haitao, Yu Bowen

Institute of Engineering Technology, University of Science and Technology Beijing, Beijing 100083, China

Abstract: Microstructure and corrosion behavior of 0.2wt% Ca and/or 0.2wt% Y modified Mg-2Zn-1Al (ZA21) rolled sheets were analyzed by SEM, XRD, hydrogen evolution and electrochemical measurement. Results show that Ca and Y refine the grains, modify the second phases, and reduce the Mn content in Mn-containing phase. In 3.5wt% NaCl solution, the preferential corrosion sites locate at the Mg-matrix near Mn-containing phases. The 12 h-corrosion rates satisfy ZA21 (8.59 mm/a)>ZA21+0.2Ca (7.17 mm/a)>ZA21+0.2Y (4.22 mm/a)>ZA21+0.2Ca+0.2Y (1.26 mm/a). The enhanced corrosion resistance of the Ca, Y modified alloys can be accredited to the follows: (1) the refinement of grain size; (2) the devitalization of the intensity of the micro-galvanic corrosion by generating low-Mn and non-Mn phases rather than the high Mn-content phases; (3) the dense, shallower cracked and more protective corrosion product film composed of Mg, $Mg(OH)_2$, Al_2O_3, Ca-containing and Y-containing components replaces the fully-cracked and limited protective one without Ca, Y incorperation.

Key words: Ca; corrosion behavior; microstructure; Y; ZA21

Mg-2Zn-1Al series magnesium alloys have been proved with balanced properties, such as Mg-2Zn-1Al-0.2Ca-0.2Gd-0.2Mn (wt%, with tensile strength of 259.6 MPa and index Erichsen (IE) value of 6.2 mm) [1] and Mg-2Zn-1Al-0.2Ca-0.2Gd (wt% , with tensile strength of 332.0 MPa and elongation of 23.1%)[2]. However, the high corrosion rates are still shortcoming for their commercial applications. As we know, the corrosion resistance of magnesium and its alloys can be severely depleted by the impurity element Fe[3,4]. Fortunately, the Mn element, an efficient purification element, is capable of binding the impurity element Fe in the Mn-containing phase, and can improve the solubility of Fe in the Mg-matrix[5]. Nevertheless, it is easier for the Mn and Al elements to form a nobler Al-Mn phase, where the micro-galvanic corrosion stimulates the corrosion of the Mg-matrix substantially[6]. Therefore, the curtailment of the Al-Mn phase present in the Mg-Al-Mn alloy seems to be instrumental in enhancing the corrosion resistance of the magnesium alloys. Therefore, changing the type, content, and distribution of Al/Mn-containing phases are essential methods to inhibit corrosion progressive[5,7,8]. It is discovered that Ca and Y elements are not only capable of enhancing the mechanical properties and the room temperature formability, but also proven to be effective decelerators of the corrosion rate. As a matter of fact, a large number of researches have been conducted on the corrosion behavior of Ca and Y elements in the Mg-Al-Zn series magnesium alloys, such as AZ91[7,9,10], AZ61[8] and AZ31[11]. The Ca-rich phases, such as Al_2Ca phase, possess a sacrificial anodic reaction than Mg matrix, thus protecting the Mg-matrix though acting as anodes[12,13]. The addition of minor Y (0.9wt%) has been proven to have a positive effect on AZ series alloys by incorporating into the layer of corrosion product[10]. Nonetheless, in most studies, an array of alloys were engineered with a concentration gradient of a certain alloying element, to examine its influence on the corrosion behavior of the alloys, while the deterioration of room temperature formability and strength caused by excessive addition of these elements was by and large overlooked[8,10,14]. Therefore, the practical application of these alloys requires the study on the influence of alloying elements on the corrosion behavior. This study aims to evaluate the corrosion rate of Mg-2Zn-1Al series alloys, and further clarify

Received date: August 02, 2021
Foundation item: Fundamental Research Funds for the Central Universities (FRF-IC-20-10)
Corresponding author: Zhang Yun, Ph.D., Assistant Research Fellow, Institute of Engineering Technology, University of Science and Technology Beijing, Beijing 100083, P. R. China, E-mail: zhangyun@ustb.edu.cn

the corrosion behavior of 0.2wt% Ca and/or 0.2wt% Y modified Mg-2Zn-1Al alloy.

1 Experiment

The composition of the Mg-2Zn-1Al series alloy is shown in Table 1. The raw materials were prepared from pure Mg (99.95wt%), pure Al (99.99wt%), pure Zn (99.99wt%), Mg-20wt% Mn, Mg-20wt% Gd, Mg-20wt% Ca and Mg-20wt% Y, and melted at 730 °C under the protection of CO_2 and SF_6 gas. Subsequently, they were cast into a corundum crucible and cooled by air. After being homogenized at 300 °C for 12 h, the ingots were rolled to 1 mm in thickness in hot rolling mill at 400 °C for several passes. Finally, the sheets with 1 mm in thickness were annealed at 350 °C for 1 h, and then cooled to room temperature by normal air.

Zeiss-Gemini 500 scanning electron microscope (SEM) was employed to observe the microstructure and corrosion morphology. The second phases were identified by energy dispersive X-ray spectroscopy (EDS) equipped in SEM. The samples were ground by SiC paper and then chemically polished in nitric acid solution (10% HNO3+90% alcohol) for 50 s, followed by etching in acetic acid solution (7%~10% acetic acid+90%~93% alcohol) for 60 s. Corrosion product identification was undertaken by employing X-ray diffraction (XRD) with a Brucker D8 Advance diffractometer. The operating voltage and current were 40 kV and 40 mA, respectively. The operating radiation was Cu Kα (λ=0.154 18 nm). The XRD patterns of the investigated alloys were tested under the diffraction angle of 10°~90°. The scanning speed was 5.8°/min with an increment of 0.02° each minute, and the results were evaluated with Jade 6 software for XRD.

Hydrogen evolution was carried out to measure the corrosion rate by chemical reaction:

$$Mg_{(s)} + 2H_2O_{(aq)} \rightarrow Mg(OH)_{2(aq)} + H_{2(g)} \quad (1)$$

According to Eq.(1), at a given time, 1 mol Mg generates 1 mol H_2. Therefore, the corrosion rate can be described as Eq.(2) by means of the hydrogen corrosion rate[15].

$$P_{H_2} = \frac{24.31V_t \times 365 \times 0.01}{22.4St\rho} = 2.08\frac{V_t}{St\rho} \quad (2)$$

where P_{H_2} (mm/a) denotes the hydrogen corrosion rate, and t (d) is the immersion time; V_t (mL) represents the hydrogen volume at a given time t; S (cm^2) indicates the area of exposed surface, and ρ (g/cm^3) is the density of investigated magnesium alloys, here ρ is 1.9 g/cm^3. The tested surface for hydrogen test with dimensions of 15 mm×20 mm was ground to 2000# by SiC paper, followed by ultrasonically vibration in 99.5% absolute ethanol for 5 min, and then instantly dried under cold air. The testing electrolyte solution was 3.5wt% NaCl aqueous solution with a pH level of 7.35. The tested temperature was 25 °C, and the immersion time for the samples was 12 h.

2 Results and Discussion

2.1 Microstructure and the second phases

The SEM morphologies of the experimental rolled sheets, ZA21, ZA21+0.2Ca, ZA21+0.2Y, and ZA21+0.2Ca+0.2Y, are shown in Fig.1, which by and large exhibit an equiaxed crystal structure with lots of blocky second phases. The microalloying elements, Ca and Y, seem to be the key contributors to the the grain size. After calculated by linear intercept method, the average grain sizes are 8.5, 7.3, 6.8 and 5.1 μm for ZA21, ZA21+0.2Ca, ZA21+0.2Y, and ZA21+0.2Ca+0.2Y sheets, respectively. Obviously, the modified sheets generate a smaller grain size as compared to the unmodified ZA21 sheets. Researches have demonstrated that Ca and Y elements are effective grain refiners, since they suitably generate the intermetallic phase to inhibit the grain growth in Mg alloys[9,16,17].

The addition of minor Ca and Y elements appropriately refines the Mg matrix and alters the form of second phases as well. The EDS spectra and corresponding element contents are shown in Fig.2 and Table 2. Clearly, Ca and Y modify the type of second phases. For ZA21 sheet, the second phases are Mg-Al-Zn-Gd and Mg-Al-Zn-Mn-Gd. For Mg-Al-Zn-Gd phase shown in Fig. 2a, the content of Al and Gd is much higher than that of Zn. The Al and Mn contents are also higher than other elements in Mg-Al-Zn-Mn-Gd phase shown in Fig.2b. For ZA21+0.2Ca sheet, the Mg-Al-Zn-Gd and Mg-Al-Zn-Mn-Gd phases still exist, and the contents of each element are similar to that in ZA21. What's more, some new Ca-containing phases, such as Mg-Al-Zn-Mn-Ca, Mg-Al-Zn-Ca and Mg-Al-Zn-Gd-Ca phases, are formed, and the Mn contents are extremely lower than that in Mg-Al-Zn-Mn-Gd phases. For ZA21+0.2Y sheets, the Mg-Al-Zn-Gd and Mg-Al-Zn-Mn-Gd still exist, but the Mn in Mg-Al-Zn-Mn-Gd phase is lower than that in ZA21. Besides, new Y-containing phases are generated, such as Mg-Al-Zn-Gd-Y, Mg-Al-Mn-Gd-Y and Mg-Al-Zn-Mn-Gd-Y, and the Mn contents in these phases are lower than that in Mg-Al-Zn-Mn-Gd phase, which means that Y can combine with Al and Mn to generate more type of phases, and decrease the content of Mn in each phase. For ZA21+0.2Ca+0.2Y sheet, the Mg-Al-Zn-Gd and Mg-Al-Zn-Mn-Gd phases disappear, Mg-Al-Zn-Ca, Mg-Al-Zn-Gd-Y, Mg-Al-Zn-Mn-Gd-Y and Mg-Al-Zn-Gd-Ca-Y are formed, and the Mn in Mg-Al-Zn-Mn-Gd-Y is lower than that in

Table 1 Chemical composition of investigated alloys (wt%)

Alloy	Zn	Al	Mn	Gd	Ca	Y	Fe
ZA21	2.01±0.45	0.99±0.36	0.18±0.11	0.14±0.05	-	-	<0.02
ZA21+0.2Ca	1.98±0.47	0.98±0.35	0.17±0.09	0.16±0.08	0.19±0.08	-	
ZA21+0.2Y	2.02±0.45	1.01±0.33	0.20±0.09	0.14±0.08	-	0.20±0.07	
ZA21+0.2Ca+0.2Y	2.00±0.46	1.02±0.35	0.20±0.08	0.15±0.07	0.19±0.08	0.22±0.08	

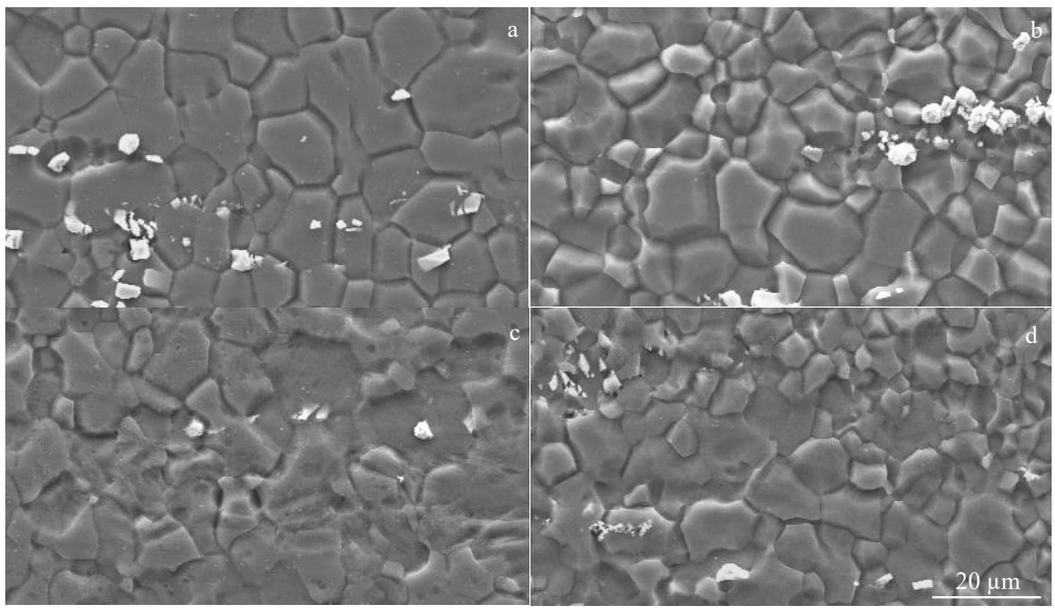

Fig.1 SEM morphologies of ZA21 (a), ZA21+0.2Ca (b), ZA21+0.2Y (c), and ZA21+0.2Ca+0.2Y (d)

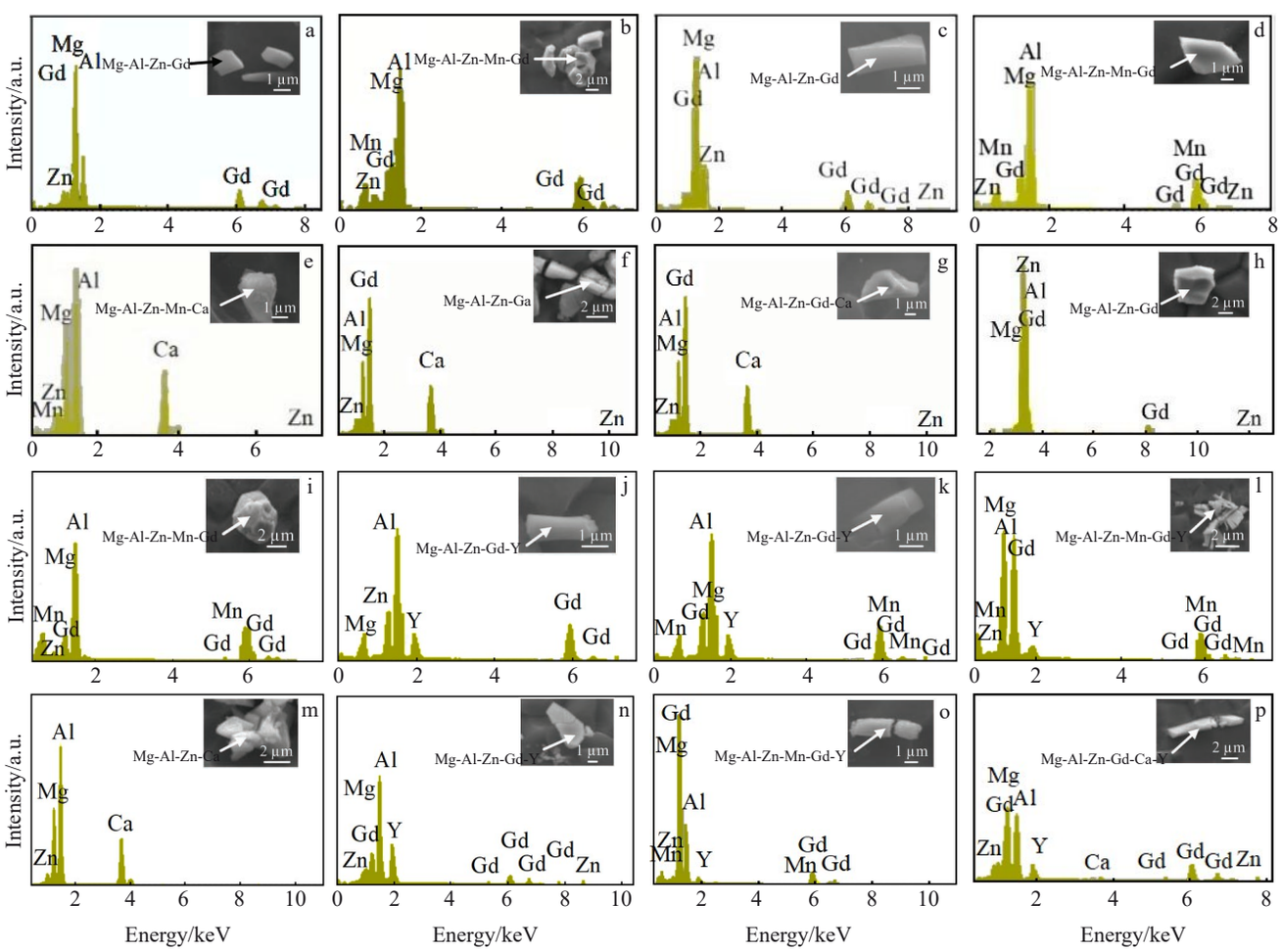

Fig.2 Second phases and corresponding EDS spectra of alloys: (a, b) ZA21; (c~g) ZA21+0.2Ca; (h~l) ZA21+0.2Y; (m~p) ZA21+0.2Ca+0.2Y

ZA21+0.2Y, which means that the inhibition of Mn-containing phases is stronger. The combination of Ca and Y can not only suppress the Mn-containing phases, but also decrease the Mn contents in Mn-containing phases.

Table 2 Element contents of second phases shown in Fig.2 (at%) obtained by EDS

Figure	Mg	Al	Zn	Mn	Gd	Ca	Y
2a	61.64	22.41	1.4	-	14.56	-	-
2b	3.07	54.11	0.83	32.76	9.23	-	-
2c	66.43	19.15	1.26	-	13.15	-	-
2d	6.62	51.47	0.83	32.58	8.5	-	-
2e	27.69	44.44	3.92	0.33	-	23.62	-
2f	16.31	54.15	4.84	-	-	24.7	-
2g	23.1	51.38	2.92	-	0.29	22.41	-
2h	81.59	11.05	0.89	-	6.49	-	-
2i	13.36	51.85	0.73	26.7	7.36	-	-
2j	72.73	16.49	1.14	-	4.49	-	5.15
2k	26.44	43.78	-	20.3	2.9	-	6.59
2l	37.29	37.64	0.66	18	3.5	-	2.9
2m	24.31	50.16	2.29	-	-	23.24	-
2n	10.88	55.3	3.6	-	11.17	-	19.04
2o	62.68	22.48	0.63	10.56	2.24	-	1.42
2p	41.34	36.42	2.67	-	13.98	0.51	5.07

2.2 Corrosion behavior

2.2.1 Hydrogen evolution

Fig. 3 shows the hydrogen volume and corresponding corrosion rate calculated by Eq. (2). The hydrogen volume curves of all the investigated sheets illustrate an increasing trend during the entire immersion process, which is an indicative of continuous corrosion reaction. The corrosion rates of the investigated alloys all sharply increase in initial immersion. As the immersion time increases, the corrosion rate decreases and gradually becomes stable. The hydrogen volume and corrosion rate show a declining order of ZA21> ZA21+0.2Ca>ZA21+0.2Y>ZA21+0.2Ca+0.2Y. The total hydrogen volume and corrosion rate of ZA21 alloy derived during the 12 h immersion is 3.92 mL/cm^2 and 8.59 mm/a, respectively. The hydrogen rates of ZA21+0.2Ca, ZA21+0.2Y, and ZA21+0.2Ca+0.2Y alloys are only 7.17, 4.22 and 1.26 mm/a, respectively. Evidently, there is a striking improvement in the corrosion resistance of the alloy sheets due to the Ca and Y addition, especially the ZA21+0.2Ca+0.2Y sheets.

2.2.2 Electrochemical analysis

Tafel and Nyquist curves after 1 h of immersion at each OCP in 3.5wt% NaCl solution are shown in Fig.4a and 4b. For Tafel curves, the investigated sheets possess different cathodic and anodic dynamics, and the corrosion potential of ZA21 sheets is found to be −1.28 V_{SCE}. The addition of Ca and Y elements tend to shift the Tafel curves to a position with less negative potential and lower corrosion current density. The improvement of E_{corr} represents the weakness of corrosion tendency, and the lower corrosion current density (i_{corr}) represents lower corrosion kinetic parameter, meaning lower corrosion rate. The i_{corr} calculated by the cathodic branch using Tafel extrapolation method (Table 3) establishes that the corrosion rate of the modified sheets is lower than that of the unmodified ones, especially ZA21+0.2Ca+0.2Y sheets, with an i_{corr} of 38.9×10^{-3} mA/cm^2. The tendency seems to be identical with the hydrogen rate shown in Fig.3b.

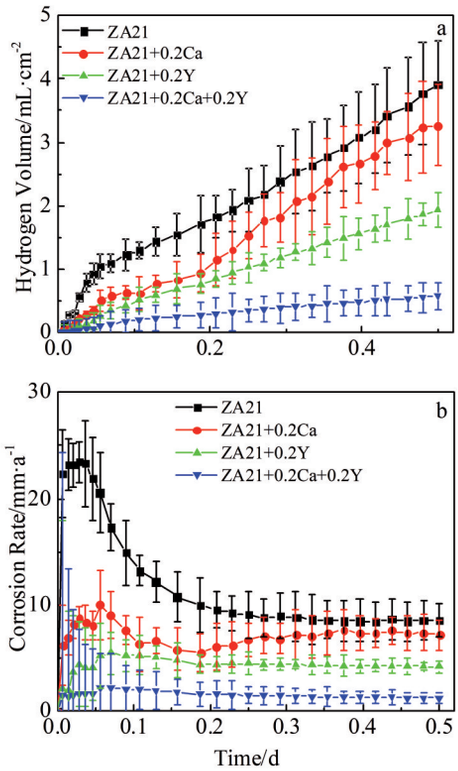

Fig.3 Hydrogen volume (a) and hydrogen corrosion rate (b) of alloys during immersion for 12 h

The Nyquist plots shown in Fig. 4b present two capacitive loops at high and medium frequency, and one inductive loop at low frequency, signifying the analogous corrosion mechanism employed by all the investigated alloys. However, the diameters of these loops appear to be dissimilar, representing different corrosion rates. The two capacitive loops are related to the electric double layer capacitor and corrosion product film. The inductive loop is associated with the breaking of corrosion product film, often accompanied by the occurrence of pitting corrosion[13,18]. The capacitive loops of all the sheets in Fig. 4b illustrate similar diameters at high frequency, but the diameters of capacitive loops at medium frequency tend to exhibit various degrees of divergence, following an increasing order of ZA21<ZA21+0.2Ca<ZA21+ 0.2Y<A21+0.2Ca+0.2Y alloy, signifying the strengthened protection effect of the corrosion product film as a result of the Y and Ca addition to the alloys.

To further analyze the electrochemical process, the equivalent circuit model was obtained and shown in Fig. 4c. After fitting the model using Z-view software, the parameters are obtained and shown in Table 4. R_s represents the solution resistance, C_{dl} denotes the electric double layer capacitor, and R_{ct} represents the charge transfer resistance. The Q and R_{film} denote the capacitance and resistance of corrosion product film, respectively. Q is a constant phase angle element,

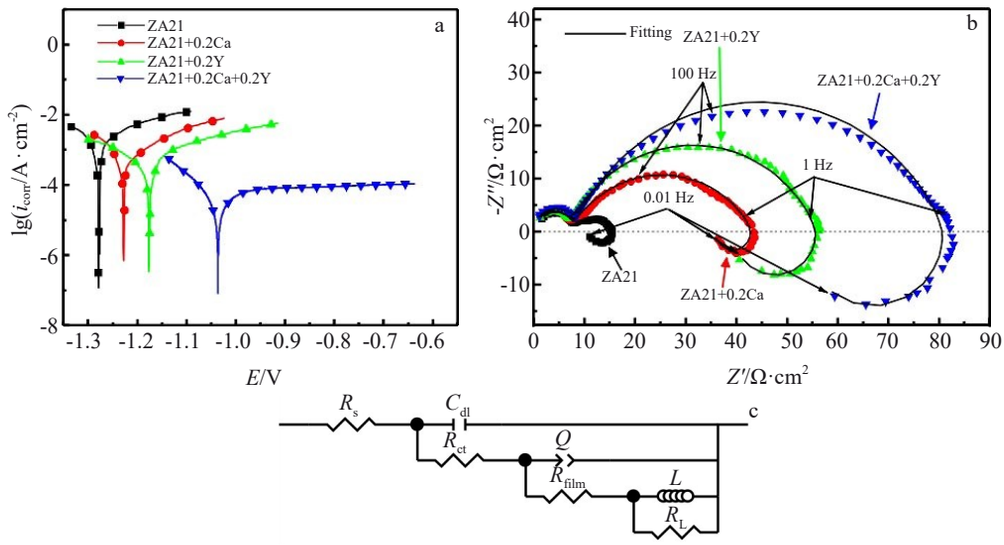

Fig.4 Tafel curves (a), Nyquist plots (b), and equivalent circuit model (c) of the alloys

Table 3 Parameters of investigated alloys extrapolated from Tafel curves

Alloy	E_{corr}/V_{SCE}	i_{corr}/×10^{-3} mA·cm^{-2}
ZA21	-1.28±0.33	1819.70±359.71
ZA21+0.2Ca	-1.23±0.31	776.25±184.44
ZA21+0.2Y	-1.18±0.28	331.13±89.45
ZA21+0.2Ca+0.2Y	-1.03±0.27	38.90±14.99

represented by parameter Y and n, and is used to replace the capacitor in non-homogenous system, while n is the dispersion coefficient, which reflects the roughness of the electrode. If n reaches the value of unity 1, Q is considered to be an ideal capacitor C. If n takes the value of 0, Q is considered to be a resistance[19,20]. The inductive component L and R_L denote inductance and resistance of inductive loops, which imply the breaking of porous $Mg(OH)_2$ film and the initiation of pitting corrosion[13,21-24]. From Fig. 4c and Table 4, it is found that R_s of the investigated alloys is not very distinctly divergent in essence, indicating an invariant immersion electrolyte condition. The C_{dl} and R_{ct} only portray slight differences. However, the R_{film} is quite distinctive, indicating the divergent protection effect of the corrosion product film. Obviously, R_{film} follows a trend of ZA21<ZA21+0.2Ca<ZA21+0.2Y<ZA21+0.2Ca+0.2Y. There fore, ZA21+0.2Ca+0.2Y possesses the optimal protective film.

2.3 Discussion

2.3.1 Effect of grain size on corrosion behavior

The above-mentioned results very lucidly illustrate that the Y and Ca elements tend to produce varying degrees of refinement effects on the grain size of ZA21 sheet, and the corrosion rates shown in Fig. 3 possess a proportional relationship with the average grain size, i.e. as the grain size decreases, the corrosion rate continues to decline. Researches have demonstrated that there are more impurities and solute atoms at the grain boundaries compared to the magnesium matrix. Thus, the more the grain boundaries, the fewer the impurity atoms in the matrix, and the more resilient the matrix [25-27].

2.3.2 Effect of second phases on corrosion behavior

The micro-galvanic corrosion between the second phases and the Mg-matrix proves to be instrumental in degenerating the corrosion resistance by promoting preferential corrosion of the Mg-matrix near second phases. Thus, the corrosion resistance can be conveniently adjusted by regulating the intensity of micro-galvanic corrosion by modifying the type, amount, size, morphology, and distribution of the second phases[5,6,11,28-31]. To analyze the effect of second phases on corrosion behavior, the investigated sheets are immersed in 3.5wt% NaCl solution for 30 s, and the corrosion morphology is observed by SEM and shown in Fig. 5. It is quite evident that a selective dissolution of the Mg-matrix occurs adjacent to the second phases. This morphology verifies the suggested

Table 4 Fitting values of circuit elements in equivalent circuit

Alloy	R_s/Ω·cm^2	C_{dl}/ ×10^{-7} F·cm^{-2}	R_{ct}/Ω·cm^2	Y/ ×10^{-4} Ω·cm^{-2}·s^n	n	R_{film}/Ω·cm^2	L/H·cm^{-2}	R_L/Ω·cm^2
ZA21	5.49±1.50	5.22±1.75	7.23±1.79	3.93±0.98	0.73±0.01	3.07±1.22	18.28±5.50	4.31±1.02
ZA21+0.2Ca	4.74±1.49	5.41±1.88	7.58±2.02	4.58±0.85	0.70±0.03	28.42±8.85	20.82±6.77	7.52±2.90
ZA21+0.2Y	4.33±1.52	4.40±1.53	7.22±1.93	1.60±0.22	0.74±0.01	32.08±9.94	90.97±18.31	16.52±7.25
ZA21+0.2Ca+0.2Y	4.05±1.45	5.02±1.67	8.31±2.21	1.67±0.19	0.75±0.02	44.69±10.00	229.00±35.50	28.19±9.42

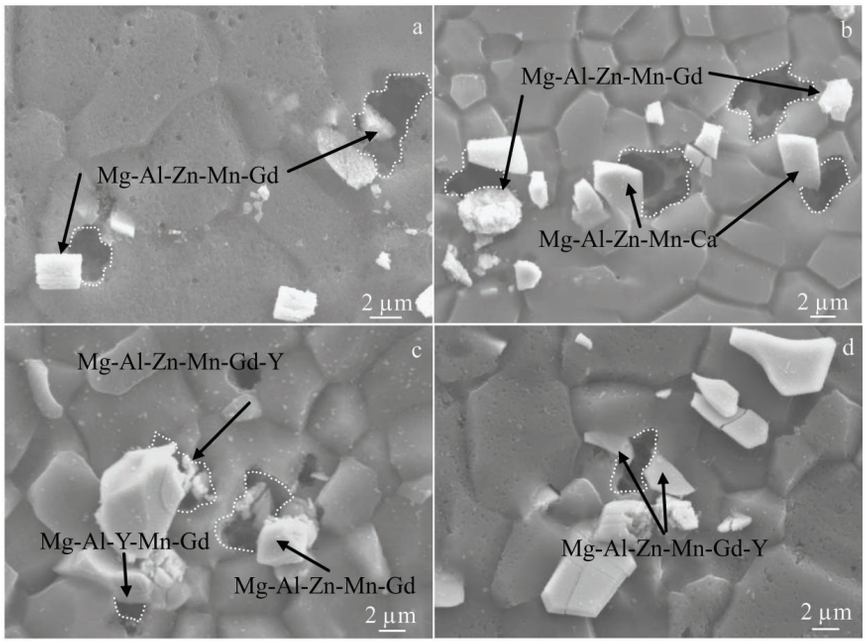

Fig.5 Corrosion morphologies of alloys after immersion for 30 s: (a) ZA21, (b) ZA21+0.2Ca, (c) ZA21+0.2Y, and (d) ZA21+0.2Ca+0.2Y

micro-galvanic corrosion mechanism of preferential dissolution of Mg-matrix near second phases caused by the positive potential differences between the second phase and the matrix. After identifying by EDS, these phases adjacent to corroded areas are all Mn-containing phase. Researchers have reported that the Mn-containing phases are nobler than Mg-matrix, such as Al_8Mn_5 phase, the potential difference with Mg-matrix is always 500 mV, and thus behaves as a strong cathode phase to accelerate the corrosion of the Mg-matrix[5,32]. Mn-containing phases dramatically deteriorate the corrosion resistance via the micro-galvanic corrosion effect. However, Ca (−2.76 V_{SCE}) and Y (−2.37 V_{SCE}) exhibit more negative standard electrode potential than Al (−1.677 V_{SCE}), Zn (−0.76 V_{SCE}), and Mn (−1.182 V_{SCE}) elements[6]. Studies have established that the potential difference between Ca-containing phase, Y-containing phase, or Gd-containing phase and the Mg-matrix is about 250, 320 and 180 mV, respectively, much lower than that of the Al-Mn phase[32-35]. According to the Mn contents calculated in Fig.2 and Table 2, the Mg-Al-Mn-Zn-Gd phases with high Mn contents gradually disappear, and the Mn contents in the newly formed Mn-containing phase, such as Mg-Al-Zn-Mn-Ca, Mg-Al-Mn-Gd-Y and Mg-Al-Zn-Mn-Gd-Y are much lower than that in Mg-Al-Mg-Gd phases. What's more, the size of corrosion pits in white dotted lines is reduced from Fig. 5a to Fig. 5d, which implies that the micro-galvanic corrosion between the Mn-containing phases and Mg-matrix is weakened, for the decreased Mn contents in Mn-containing phases. Further, the corrosion rates are also proportional to the Mn contents in Mn-containing phases, which demonstrates that the deterioration of Mg-matrix by Mn-containing phases decreases with the addition of Ca and Y.

2.3.3 Protection of the corrosion product film

$Mg(OH)_2$ happens to be the main component of corrosion product film; however, it proves to be an unsuitable passive film for the prevention of corrosion outbreak due to its porous nature and the lower Pilling-Bedworth ratio (0.81)[36]. Alloying can significantly modify the integrity and density of the corrosion product film. An integrity and dense film is capable of effectively safeguarding the matrix from a corrosion outbreak[15]. Fig. 6 shows the surface morphologies, cross-section morphologies and corresponding XRD patterns of the investigated sheets after immersion for 12 h. The corrosion product films of the four alloys are covered with varying degrees of cracks, and the magnified morphologies are all honeycomb, indicating that the addition of trace Ca and Y does not modify the structure of corrosion product. But the cracks decrease with the addition of Ca and Y, especially the ZA21+0.2Ca+0.2Y sheet. The cross section of ZA21 exhibits an uneven oxide film with many cracks, which is indicative of limited protection. The integrity of the film of ZA21+0.2Ca alloy does not change to a great extent qualitatively, but the flatness of the film has been improved to a certain extent judging from the cross-sectional morphology, indicating more homogeneous film. The ZA21+0.2Y alloy exhibits a film with narrower cracks, and there are no obvious cracks in cross section. However, there are still bulges on the exposed surface. The bulge-shaped protective film seems easy to fall off, which weakens the protective effect of the film on the Mg-matrix[35]. The ZA21+0.2Ca+0.2Y sheet possesses the densest and least cracked film, as shown in Fig. 6d, and the cross section performs a flatter and denser film, which possesses the most protective effect to prevent the matrix from corrosion attacking. Moreover, the morphologies of product films are in good agreement with the R_{film} calculated in Nyquist plot.

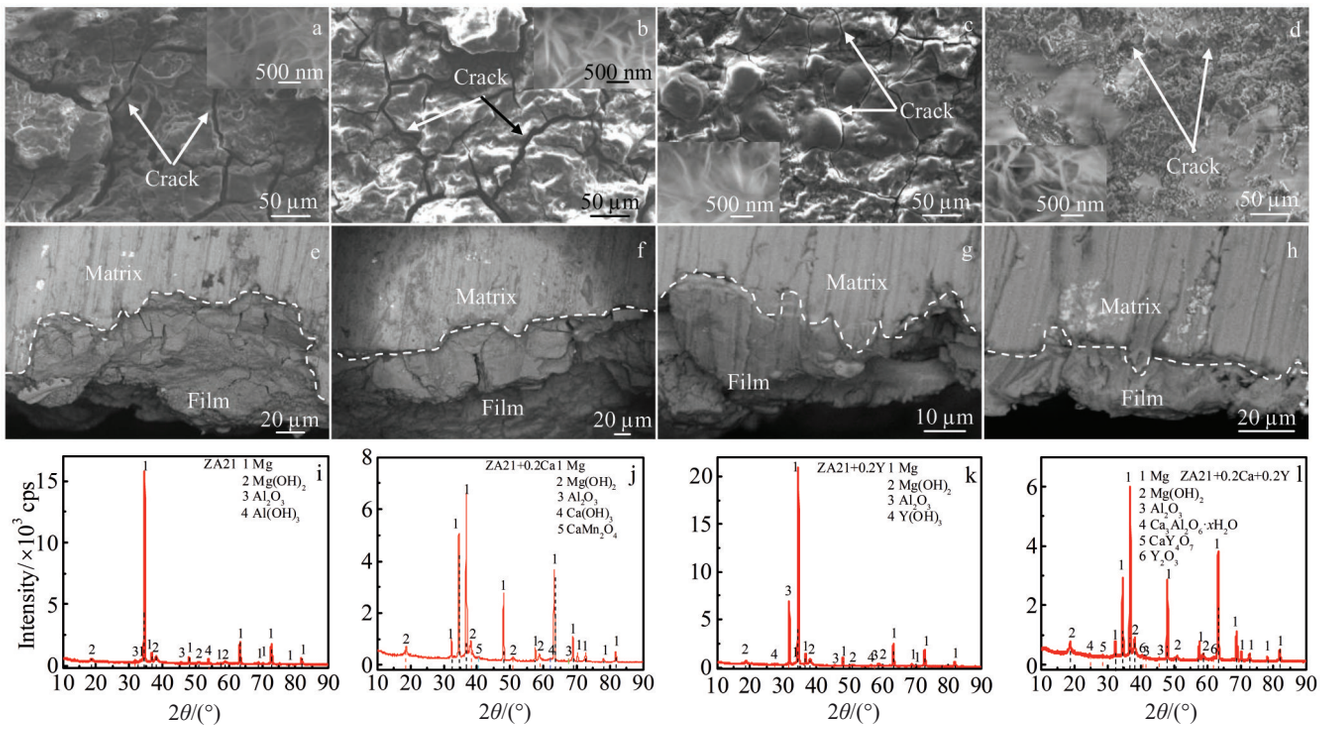

Fig.6 Corroded surfaces (a~d), cross-section morphologies (e~h) and XRD patterns (i~l) of corrosion product film: (a, e, i) ZA21, (b, f, j) ZA21+0.2Ca, (c, g, k) ZA21+0.2Y; (d, h, l) ZA21+0.2Ca+0.2Y

The XRD diffraction patterns of the corrosion product films indicate that Mg and $Mg(OH)_2$ are the dominant corrosion product, and the peaks of Al_2O_3 are also detected in all investigated alloys. Besides, for ZA21 alloys, $Al(OH)_3$ is also identified, Al-containing film has been proved to have an excellent protection due to its dense nature; however, the peaks of Al-containing product are too small to provide enough protection to the matrix against corrosion attacking, thus the corrosion product film still maintains the poor nature of $Mg(OH)_2$. The $Ca(OH)_2$ and $CaMn_2O_4$ are also detected in ZA21+0.2Ca alloy. Studies have demonstrated that the addition of Ca element is conducive to the improvement in the continuity of the magnesium alloy film, thereby providing an enhanced protection of the film to the matrix [11,37]. The XRD pattens in ZA21+0.2Y actually prove the presence of Y-containing hydroxide. The addition of Y to Mg alloys can also generate Y_2O_3 protective film, reducing the cathode current density and increasing the alloy corrosion resistance [38]. Besides the peaks of Mg, $Mg(OH)_2$ and Al_2O_3 are observed, $Ca_3Al_2O_6{\cdot}xH_2O$, CaY_4O_7 and Y_2O_3 peaks are identified in ZA21+0.2Ca+0.2Y alloy, which means that Ca and Y elements both contribute to the dense product film. According to Woo et al [39], Y added to the Ca-containing AZ91 magnesium alloy can achieve a more stable surface film, delay the rupture of the film, and thereby increase the corrosion resistance of the alloy. In other words, although trace Ca and Y do not change the structure of the corrosion product film, they reduce the cracks of the film, increase the flatness and integrity, and thus enhance the protection of the film.

3 Conclusions

1) Ca and Y addition can refine the grain size and modify the second phases of ZA21 sheets. The grain sizes of ZA21, ZA21+0.2Ca, ZA21+0.2Y and ZA21+0.2Ca+0.2Y are 8.5, 7.3, 6.8 and 5.1 μm, respectively. The addition of 0.2wt% Ca and 0.2wt% Y can not only suppress the high Mn-containing phases, but also decrease the Mn contents in Mn-containing phases.

2) The corrosion resistance follows the order by a declining trend: ZA21+0.2Ca+0.2Y (1.26 mm/a) >ZA21+0.2Y (4.22 mm/a) >ZA21+0.2Ca (7.17 mm/a) >ZA21 (8.59 mm/a). The corrosion attack commences in the Mg-matrix in the vicinity of the Mn-containing phases.

3) 0.2wt% Ca and 0.2wt% Y have positive effects on the corrosion resistance of ZA21 sheet due to the refinement of grain size, the lower micro-galvanic corrosion intensity between second phases and Mg-matrix and the more protective film composed of Ca-, Y-containing components.

References

1 Zhang Y, Jiang H T, Wang S H *et al. Materials Science and Engineering A*[J], 2021, 804: 140 566

2 Niu Y X, Song Z T, Le Q C *et al. Journal of Alloys and Compounds*[J], 2019, 801: 415

3 Wang Y N, Zhang Y Z, Hou L F *et al. Rare Metal Materials and Engineering*[J], 2021, 50(1): 49 (in Chinese)

4 Shi Z M, Cao F Y, Song G L *et al. Corrosion Science*[J], 2013,

76: 98
5 Metalnikov P, Hamu G B, Templeman Y *et al. Materials Characterization*[J], 2018, 145: 101
6 Mingo B, Arrabal R, Mohedano M *et al. Materials Design*[J], 2017, 130: 48
7 Wang Y Q, Li M Z, Li C *et al. Materials and Corrosion*[J], 2012, 63: 497
8 Manivannan S, Dinesh P, Kumaresh Babun S P *et al. Journal of Magnesium and Alloys*[J], 2015, 3: 86
9 Wu G Y, Fan Y, Gao H T *et al. Materials Science and Engineering A*[J], 2005, 408: 255
10 Jia R L, Zhang M, Zhang L N *et al. Journal of Alloys and Compdounds*[J], 2015, 634: 263
11 Zhang C, Wu L, Huang G S *et al. Journal of the Electrochemical Society*[J], 2019, 166: 445
12 Südholz A, Kirkland N, Buchheit R *et al. Electrochemical and Solid-State Letters*[J], 2011,14(2): 5
13 Yang J, Peng J, Nyberg E A *et al. Applied Surface Science*[J], 2016, 369: 92
14 Gateman S M, Georgescu N S, Kim M K *et al. Journal of the Electrochemical Society*[J], 2019, 166: 624
15 Shi Z M, Liu M, Andrej A. *Corrosion Science*[J], 2010, 52: 579
16 Lee Y C, Dahl A K, StJohn D H. *Metalluigical and Materials Transactions A*[J], 2000, 31: 2895
17 Chen R, Xu J Y, Zhang D F *et al. Rare Metal Materials and Engineering*[J], 2019, 48(7): 2084 (in Chinese)
18 Wang H X, Song Y W, Yu J *et al. Journal of the Electrochemical Society*[J], 2017, 164: 574
19 Li C Q, Xu D K, Zeng Z R *et al. Materials and Design*[J], 2017, 121: 430
20 Wang Y J, Zhang Y, Wang P P *et al. Journal of Materials Research and Technology*[J], 2020, 9: 7087
21 Song Y W, Shan D Y, Chen R S *et al. Corrosion Science*[J], 2009, 51: 1087
22 King A D, Birbilis N, Scully J R. *Electrochima Acta*[J], 2014, 121: 394
23 Ke C, Wu Y J, Qiu Y *et al. Corrosion Science*[J], 2016, 113: 145
24 Li C Q, Xu D K, Chen X B *et al. Electrochimica Acta*[J], 2018, 260: 55
25 Song G L, Xu Z Q. *Corrosion Science*[J], 2012, 54: 97
26 Liu M, Uggowitzer P J, Nagasekhar A V *et al. Corrosion Science* [J], 2009, 51(3): 602
27 Liu M, Song G L. *Corrosion Science*[J], 2013, 77: 143
28 Cao F Y, Shi Z M, Song G L *et al. Corrosion Science*[J], 2015, 90: 176
29 Zhang C, Wu L, Liu H *et al. Corrosion Science*[J], 2020, 174: 108 831
30 Esmaily M, Svensson J E, Fajardo S *et al. Progress in Materials Science*[J], 2017, 89: 92
31 Li L, Nam N D. *Journal of Magnesium and Alloys*[J], 2016, 4: 44
32 Baek S M, Kim H J, Jeong H Y *et al. Corrosion Science*[J], 2016, 112: 44
33 Gong C W, He X Z, Yan X. *Journal of Physics and Chemistry of Solids*[J], 2021,152: 109 952
34 Baek S M, Kang J S, Shin H J *et al. Corrosion Science*[J], 2017, 118: 227
35 Arrabal R, Pardo A, Merino M C *et al. Corrosion*[J], 2012, 68(5): 398
36 Zeng R C, Sun L, Zheng Y F *et al. Corrosion Science*[J], 2014, 79: 69
37 Zhang C, Wu L, Huang G S *et al. Journal of Alloys and Compounds*[J], 2020, 823: 153 844
38 Yu X W, Jiang B, He J J *et al. Journal of Alloys and Compounds* [J], 2018, 749: 1054
39 Woo S K, Blawert C, Yasakau K A *et al. Corrosion Science*[J], 2020, 166: 108 451

Ca、Y改性的Mg-2Zn-1Al镁合金腐蚀行为

王玉娇，张　韵，江海涛，于博文
(北京科技大学 工程技术研究院，北京 100083)

摘　要：采用扫描电镜、XRD、析氢及电化学测试等对0.2%Ca、0.2%Y改性的Mg-2Zn-1Al（ZA21）轧制板材的微观组织和腐蚀行为进行了分析。结果表明，Ca和Y细化了晶粒，改变了第二相类型，降低了含Mn相中锰含量。在3.5%NaCl溶液中，优先腐蚀位点位于含Mn相附近的镁基体上，12 h腐蚀速率满足：ZA21 (8.59 mm/a)>ZA21+0.2%Ca (7.17 mm/a)>ZA21+0.2%Y (4.22 mm/a)>ZA21+0.2%Ca+0.2%Y (1.26 mm/a)。耐蚀性提升可归因于晶粒的细化；高Mn相消失，低Mn相和无Mn相生成导致微电偶腐蚀减弱；Mg、$Mg(OH)_2$、$Ca_3Al_2O_6{\cdot}xH_2O$、CaY_4O_7和Y_2O_3组成的更致密、裂纹更浅、保护性更强的腐蚀产物膜替代了由Mg和$Mg(OH)_2$组成的充满裂纹、保护作用有限的腐蚀产物膜。

关键词：Ca；腐蚀行为；微观组织；Y；ZA21

作者简介：王玉娇，女，1993年生，博士生，北京科技大学工程技术研究院，北京 100083，E-mail：wangyujiao_2018@126.com